

Magnetic-field and current-density distributions in thin-film superconducting rings and disks

Ali A. Babaei Brojeny

*Department of Physics, Isfahan University of Technology,
Isfahan 84154, Iran, and Department of Physics and Astronomy,
Iowa State University, Ames, Iowa, 50011-3160*

John R. Clem

*Ames Laboratory and Department of Physics and Astronomy,
Iowa State University, Ames, Iowa, 50011-3160*

(Dated: May 1, 2019)

We show how to calculate the magnetic-field and sheet-current distributions for a thin-film superconducting annular ring (inner radius a , outer radius b , and thickness $d \ll a$) when either the penetration depth obeys $\lambda < d/2$ or, if $\lambda > d/2$, the two-dimensional screening length obeys $\Lambda = 2\lambda^2/d \ll a$ for the following cases: (a) magnetic flux $\Phi_z(a)$ trapped in the hole in the absence of an applied magnetic field, (b) zero magnetic flux in the hole when the ring is subjected to an applied magnetic field H_a , and (c) focusing of magnetic flux into the hole when a magnetic field H_a is applied but no net current flows around the ring. We use a similar method to calculate the magnetic-field and sheet-current distributions and magnetization loops for a thin, bulk-pinning-free superconducting disk (radius b) containing a dome of magnetic flux of radius a when flux entry is impeded by a geometrical barrier.

PACS numbers: 74.78.-w, 74.25.Ha, 74.25.Op, 74.25.-q

I. INTRODUCTION

Recently Babaei Brojeny et al.¹ reported exact analytical solutions for the magnetic-field and sheet-current-density profiles for two current-carrying parallel coplanar thin-film superconducting strips in a perpendicular magnetic field. Included were calculations for (a) the inductance per unit length when the two strips carry equal and opposite currents, (b) the zero-flux-quantum state when no net magnetic flux threads between the strips in a perpendicular applied field H_a , and (c) the focusing of magnetic flux between the two strips in a field H_a when each strip carries no net current. These problems are of relevance to the design of superconducting thin-film devices, especially superconducting quantum interference devices (SQUIDs).

Of interest is the focusing of magnetic flux into the central hole in washer-type² SQUIDs and, in particular, the question of how much flux Φ_h goes into the hole when the SQUID is in a perpendicular magnetic field $H_a = B_a/\mu_0$ and no net current circulates around the hole. The flux-focusing problem was examined by Ketchen et al.,³ who expressed Φ_h in terms of an effective pickup area of the hole, $A_{eff} = \Phi_h/B_a$, which in general is larger than the actual area of the hole, A_h , but less than the area occupied by the washer, A_w . Accounting only for azimuthal currents, they considered a washer of circular geometry (an annular ring) and derived a simple theoretical expression for the effective area, $A_{eff} \approx (8/\pi^2)A_h(A_w/A_h)^{1/2}$, the theoretical approximations used being valid only for $A_h \ll A_w$. Experiments on a series of square washers with A_w/A_h up to 10^4 yielded results in excellent qualitative agreement with the prediction, but with

$$A_{eff} \approx 1.1A_h(A_w/A_h)^{1/2}.$$

Experiments by Dantsker et al.⁴ on SQUIDs made with narrow superconducting lines separated by slots or holes (for trapping flux quanta during cooldown in the earth's magnetic field) have revealed that the presence of slots or holes increases the effective area over the value for a solid washer. This effect was confirmed experimentally by Jansman et al.,⁵ who were able to account for the increased effective area by treating the slotted washers as parallel circuits of pickup inductances.

In this paper we introduce an approach suitable for extension to calculations of the magnetic-field and sheet-current-density distributions in superconducting thin-film strips, rings, and narrow lines. We consider the idealized case for which the penetration depth λ obeys $\lambda < d/2$ or, if $\lambda > d/2$, the two-dimensional screening length $\Lambda = 2\lambda^2/d$ obeys $\Lambda \ll a$, such that the key boundary condition is that the normal component of the magnetic induction is zero on the surface of the superconductor. A complicating consequence is that the sheet-current distribution in the superconductor has inverse square-root singularities at the edges. While a mutual-inductance approach such as that used by Gilchrist and Brandt⁶ and Jansman et al.⁵ is always applicable, we show here that an approach taking into account the inverse-square-root singularities from the beginning is simpler and more efficient.

The authors of Ref. 3 obtained the flux-focusing result by superposition. They first calculated the induced current flowing in the clockwise direction in an applied magnetic induction B_a assuming zero magnetic flux in the hole. They approximated this current using the known result for a superconducting disk with no central hole.

They next calculated the induced current flowing in the counterclockwise direction in the absence of an applied field assuming a given amount of magnetic flux Φ_h in the hole. They approximated this current using the known result for an infinite superconducting sheet with a round hole in it. Finally they obtained the relation between B_a and Φ_h by equating the magnitudes of the two circulating currents. In the present paper, we show how to calculate all properties without making the small-hole approximations used in Ref. 3. We show how to solve the flux-focusing problem directly, as well as by superposition.

Another problem of interest is the calculation of the magnetic-field and current-density distribution for the case of a bulk-pinning-free type-II superconducting disk of radius b and thickness $d \ll b$ in which the entry of magnetic flux is impeded by a geometrical barrier.^{7,8} Analytic solutions for the field and current distributions and the magnetization in strips subject to a geometrical barrier have been studied for the bulk-pinning-free case in Refs. 9 and 10 and for the case of Bean-model bulk pinning ($J_c = \text{const}$) in Ref. 11. Numerical results for the field and current distributions and the magnetization in disks subject to both a geometrical barrier and bulk pinning with a B -dependent J_c have been presented in Ref. 12. In the following, we present an efficient method for calculating the field and current distributions and the magnetization in bulk-pinning-free disks subject to a geometrical barrier.

Our paper is organized as follows. In Sec. II, we outline our approach and set down the basic equations. In Sec. III, we apply this approach to calculate the inductance of an annular ring of arbitrary inner radius. In Sec. IV, we calculate the current circulating around a ring remaining in the zero-flux-quantum state while subjected to a perpendicular magnetic field. In Sec. V, we consider the flux-focusing problem and calculate the magnetic flux contained in the center of a ring in an applied magnetic field when there is no net current around the ring. In Sec. VI, we calculate the magnetization loop for a bulk-pinning-free thin-film type-II superconducting disk subject to a geometrical barrier. We briefly discuss our results in Sec. VII.

II. BASIC EQUATIONS

We consider a thin-film superconducting annular ring in the plane $z = 0$, centered on the z axis, with inner and outer radii a and b and thickness $d \ll a$. We assume that either $\lambda < d/2$ or $\Lambda \ll a$ if $\lambda > d/2$, as discussed in the introduction. By the Biot-Savart law, the z component of the magnetic field in the plane $z = 0$ is^{13,14}

$$H_z(\rho) = H_a + \frac{1}{2\pi} \int_a^b G(\rho, \rho') K_\phi(\rho') d\rho', \quad (1)$$

where H_a is the applied field, $K_\phi(\rho)$ is the sheet-current density in the counterclockwise direction,

$$G(\rho, \rho') = K(k)/(\rho + \rho') - E(k)/(\rho - \rho'), \quad (2)$$

$$k = 2(\rho\rho')^{1/2}/(\rho + \rho'), \quad (3)$$

and K and E are complete elliptic integrals of the first and second kind with modulus k . An important boundary condition we will use in this paper is that $H_z(\rho) = 0$ for $a < \rho < b$. The total current in the counterclockwise direction is

$$I = \int_a^b K_\phi(\rho) d\rho, \quad (4)$$

and the magnetic moment along the z direction is

$$m_z = \pi \int_a^b \rho^2 K_\phi(\rho) d\rho. \quad (5)$$

Another quantity of interest is the magnetic flux up through a circle of radius ρ in the plane $z = 0$,^{13,14}

$$\Phi_z(\rho) = \mu_0 H_a \pi \rho^2 + \frac{\mu_0}{2} \int_a^b G_A(\rho, \rho') K_\phi(\rho') d\rho', \quad (6)$$

where

$$G_A(\rho, \rho') = (\rho + \rho')[(2 - k^2)K(k) - 2E(k)] \quad (7)$$

and k is given in Eq. (3).

In the following sections we present solutions of the above equations and determine the corresponding sheet-current density $K_\phi(\rho)$ for four cases: (a) self-inductance $L = \Phi_z(a)/I$ when $H_a = 0$, (b) the zero-flux-quantum state [$\Phi_z(a) = 0$] in an applied field H_a , (c) flux focusing in an applied field [calculation of $\Phi_z(a)$ when $I = 0$], and (d) geometrical-barrier effects in a thin disk of radius b containing a Lorentz-force-free magnetic-flux dome of radius a . In each case, we assume a spatial dependence of the reduced sheet-current density of the form

$$\tilde{K}_\phi(u) = \frac{4g(u)}{\pi u \sqrt{(u^2 - \tilde{a}^2)(1 - u^2)}}, \quad (8)$$

where $u = \rho/b$ and $\tilde{a} = a/b$ and $g(u)$ is a polynomial containing N terms,

$$g(u) = \sum_{m=1}^N g_m \left(\frac{u - \tilde{a}}{1 - \tilde{a}} \right)^{m-1}. \quad (9)$$

Although we are not certain that such a choice gives an exact solution in general, it reduces to known exact solutions in various limits [$a \rightarrow 0$, $b \rightarrow \infty$, or $(b - a) \ll b$], all of which have inverse-square-root singularities at the sample edges. To determine the N coefficients, $N - 1$ equations are obtained by setting $H_z(\rho_n) = 0$, where

$\rho_n = a + n(b - a)/N$ and $n = 1, 2, \dots, N - 1$. The N -th equation depends on the case under consideration; for case (a) we use Eq. (4) for given I , for case (b) we use Eq. (6) and set $\Phi_z(a) = 0$, for case (c) we use Eq. (4) and set $I = 0$, and for case (d) we use Eq. (9) and set $g(\tilde{a}) = 0$.

For numerical evaluation of the integrals in Eqs. (1), (4), (5), and (6), it is convenient to change variables using the substitution $v = \rho'/b = \sqrt{\tilde{a}^2 + (1 - \tilde{a}^2) \sin^2 \phi}$ and to define the functions

$$h_m(u) = \frac{2}{\pi^2} \int_0^{\pi/2} G(u, v) \left(\frac{v - \tilde{a}}{1 - \tilde{a}} \right)^{m-1} v^{-2} d\phi, \quad (10)$$

$$i_m = \frac{4}{\pi} \int_0^{\pi/2} \left(\frac{v - \tilde{a}}{1 - \tilde{a}} \right)^{m-1} v^{-2} d\phi, \quad (11)$$

$$f_m = \frac{4}{\pi} \int_0^{\pi/2} \left(\frac{v - \tilde{a}}{1 - \tilde{a}} \right)^{m-1} d\phi, \quad (12)$$

$$\phi_m(u) = \frac{2}{\pi} \int_0^{\pi/2} G_A(u, v) \left(\frac{v - \tilde{a}}{1 - \tilde{a}} \right)^{m-1} v^{-2} d\phi, \quad (13)$$

and

$$\alpha_{nm} = h_m(u_n), \quad (14)$$

where $u_n = \rho_n/b = \tilde{a} + n(1 - \tilde{a})/N$, and $n = 1, 2, \dots, N - 1$. For $a < \rho < b$ ($\tilde{a} < u < 1$), Eqs. (10) and (13) are principal-value integrals, evaluated by splitting the ϕ integral into two parts, one from 0 to $\Phi(u - \epsilon)$ and the other from $\Phi(u + \epsilon)$ to $\pi/2$, where

$$\Phi(u) = \sin^{-1} \sqrt{\frac{u^2 - \tilde{a}^2}{1 - \tilde{a}^2}} \quad (15)$$

and ϵ is an infinitesimal. For the results presented here we have used $\epsilon = 10^{-7}$.

III. INDUCTANCE OF AN ANNULAR RING

To calculate the inductance, we set $H_a = 0$ in Eq. (1) and define $K_{I\phi} = (I_I/b)\tilde{K}_{I\phi}$, where the subscript I henceforth labels all quantities that are specific to calculations of the inductance. To evaluate the coefficients g_{Im} in

$$g_I(u) = \sum_{m=1}^N g_{Im} \left(\frac{u - \tilde{a}}{1 - \tilde{a}} \right)^{m-1}, \quad (16)$$

we use the N equations

$$\sum_{m=1}^N \alpha_{Imm} g_{Im} = \beta_{In}, \quad (17)$$

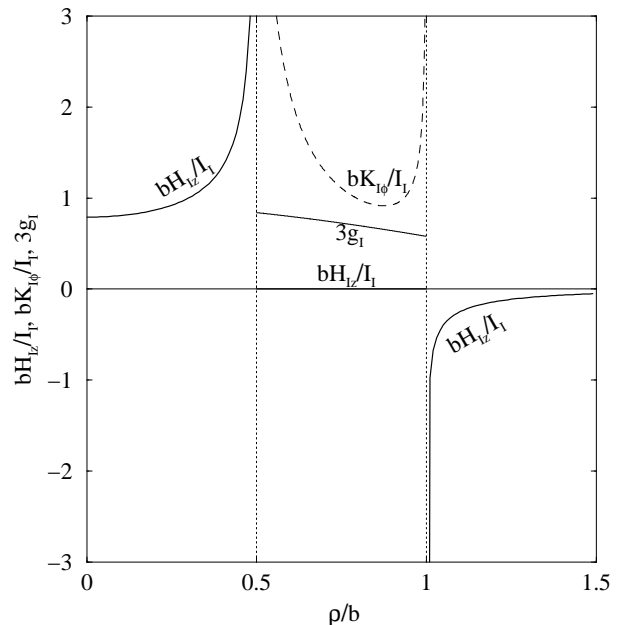


FIG. 1: Reduced magnetic field $\tilde{H}_{Iz} = bH_{Iz}/I_I$, reduced sheet-current density $\tilde{K}_{I\phi}$, and polynomial g_I (multiplied by 3) vs $u = \rho/b$ obtained while calculating the inductance for a superconducting ring with $\tilde{a} = a/b = 0.5$.

$n = 1, 2, \dots, N$, where $\alpha_{Inm} = \alpha_{nm}$ and $\beta_{In} = 0$ for $n < N$, and $\alpha_{INm} = i_m$ and $\beta_{IN} = 1$ for $n = N$. These equations are obtained from Eqs. (1), (8), (9), (10), and (14) and $H_z(\rho_n) = 0$ for $n < N$, and from Eqs. (4), (8), (9), and (11) for $n = N$.

Numerical results for $\tilde{H}_{Iz} = bH_{Iz}/I_I$, $\tilde{K}_{I\phi}$, and g_I vs $u = \rho/b$ for $a = b/2$ ($\tilde{a} = 0.5$) are shown in Fig. 1. In this calculation, as well as in all others in Secs. III-VI, the magnitude of the reduced magnetic field for $a < \rho < b$ was less than 10^{-5} except for ρ very close to a or b , where the numerical results for the principal-value integrals in Eq. (10) became less accurate. Results for g_{Im} vs \tilde{a} are shown in Fig. 2. The inductance is calculated from

$$L = \Phi_{Iz}/I_I = \mu_0 b \tilde{\Phi}_{Iz}(\tilde{a}), \quad (18)$$

where

$$\tilde{\Phi}_{Iz}(u) = \sum_{m=1}^N \phi_m(u) g_{Im}, \quad (19)$$

and is shown in Fig. 3 as a function of $\tilde{a} = a/b$. Dashed lines in Fig. 3 show expressions valid in the limits of small and large \tilde{a} : For $\tilde{a} \ll 1$, the inductance approaches $L_0 = 2\mu_0 a$ [or $\tilde{\Phi}_{Iz}(\tilde{a}) = 2\tilde{a}$], as obtained by Ketchen et al.,³ and for $\tilde{a} \rightarrow 1$, the inductance approaches

$$L_1 = \mu_0 R [\ln(8R/w) - (2 - \ln 4)], \quad (20)$$

as obtained by Brandt¹⁵ for a superconducting annulus of mean radius R and width $w \ll R$. [Here $R = (a +$

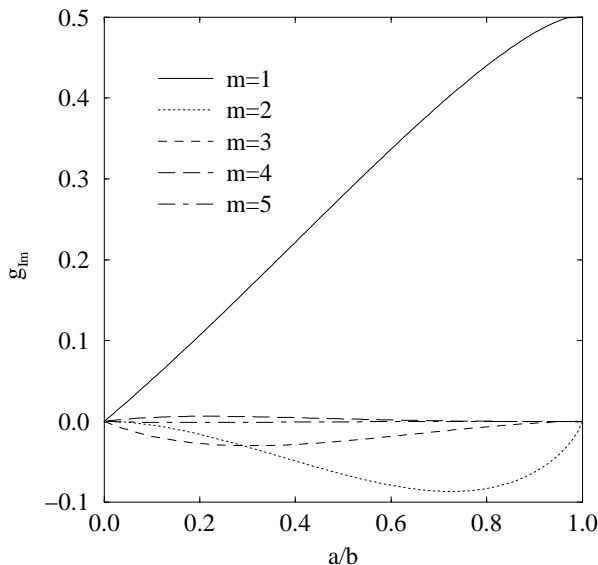


FIG. 2: Coefficients g_{Im} in the polynomial of Eq. (16) vs $\tilde{a} = a/b$ obtained while calculating the inductance of a superconducting ring.

$b)/2 = b(1 + \tilde{a})/2$ and $w = (b - a) = b(1 - \tilde{a})$.] Equation (20) can be obtained from¹⁶ $L = \mu_0 R [\ln(8R/r) - 2]$, the inductance of a superconducting ring of radius R and wire radius $r \ll R$, by replacing r by $w/4$.¹⁷ The empirical formula

$$L_2 = \mu_0 b [\tilde{a} - 0.197\tilde{a}^2 - 0.031\tilde{a}^6 + (1 + \tilde{a}) \tanh^{-1} \tilde{a}], \quad (21)$$

where $\tilde{a} = a/b$, fits our numerical results for L within 0.06%, and a plot of it is indistinguishable from the solid curve in Fig. 3.

The magnetic moment associated with the circulating current can be calculated from

$$m_{Iz} = I_I \pi b^2 \sum_{m=1}^N f_m g_{Im}. \quad (22)$$

IV. ZERO-FLUX-QUANTUM STATE

Consider an annular ring that has been cooled into the superconducting state in the absence of a magnetic field, such that no magnetic flux is trapped anywhere in the ring. When a perpendicular magnetic field H_a is applied, a circulating current is induced, but the ring remains in the Meissner state, and the magnetic flux up through the hole remains zero (there are no flux quanta in the hole). The induced sheet current density is $K_{Z\phi} = H_a \tilde{K}_{Z\phi}$, where the subscript Z henceforth labels all quantities that are specific to calculations for the zero-flux-quantum state. To evaluate the coefficients g_{Zm} in

$$g_Z(u) = \sum_{m=1}^N g_{Zm} \left(\frac{u - \tilde{a}}{1 - \tilde{a}} \right)^{m-1}, \quad (23)$$

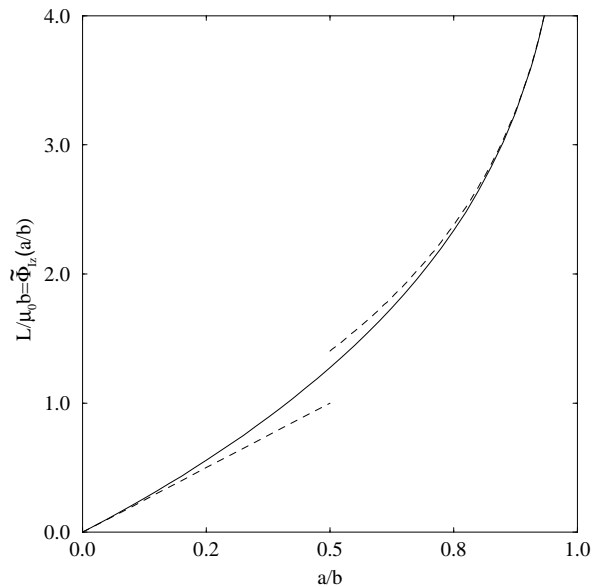


FIG. 3: Reduced inductance of a superconducting ring, $L/\mu_0 b$ vs $\tilde{a} = a/b$, calculated from Eqs. (18) and (19). Dashed curves show approximations valid in the limits $\tilde{a} \rightarrow 0$ and $\tilde{a} \rightarrow 1$.

we use the N equations

$$\sum_{m=1}^N \alpha_{Znm} g_{Zm} = \beta_{Zn}, \quad (24)$$

$n = 1, 2, \dots, N$, where $\alpha_{Znm} = \alpha_{nm}$ and $\beta_{Zn} = -1$ for $n < N$, and $\alpha_{ZNm} = \phi_m(\tilde{a})$ and $\beta_{ZN} = -\pi \tilde{a}^2$ for $n = N$. These equations are obtained from Eqs. (1), (8), (9), (10), and (14) and $H_z(\rho_n) = 0$ for $n < N$, and from Eqs. (6), (8), (9), and (13) for $n = N$.

Numerical results for $\tilde{H}_{Zz} = H_{Zz}/H_a$, $\tilde{K}_{Z\phi}$, and g_Z vs $u = \rho/b$ for $a = b/2$ ($\tilde{a} = 0.5$) are shown in Fig. 4. Results for g_{Zm} vs \tilde{a} are shown in Fig. 5. The magnitude $|I_Z|$ of the induced current is obtained from $I_Z = H_a b \tilde{I}_Z$, where

$$\tilde{I}_Z = \sum_{m=1}^N i_m g_{Zm}, \quad (25)$$

and is shown in Fig. 6 as a function of $\tilde{a} = a/b$. Dashed lines in Fig. 6 show expressions valid in the limits of small and large \tilde{a} : For $\tilde{a} \ll 1$, the induced current approaches $I_Z = -4H_a b/\pi$ [or $\tilde{I}_Z = -4/\pi$], as obtained by Ketchen et al.,³ and for $\tilde{a} \rightarrow 1$, the induced current approaches $I_Z = -\pi R^2 B_a/L_1$.

V. FLUX FOCUSING

We now solve for the current and field distribution when a superconducting annular ring is placed in a perpendicular magnetic field H_a subject to the condition that there is no net current circulating around the ring.

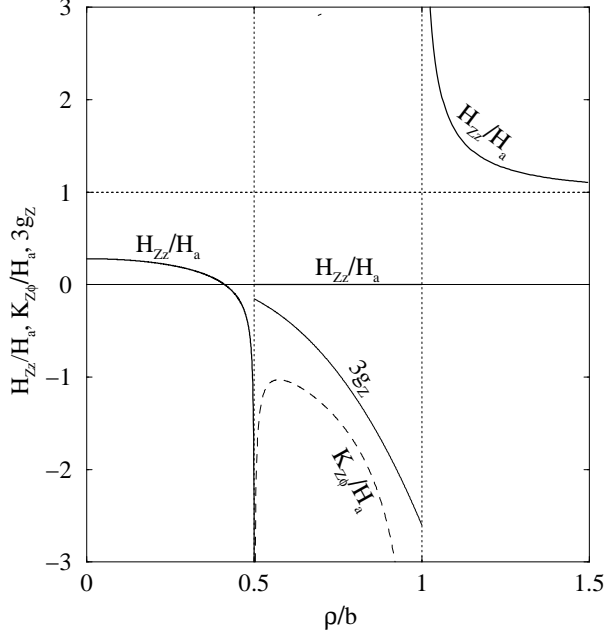


FIG. 4: Reduced magnetic field $\tilde{H}_{Zz} = H_{Zz}/H_a$, reduced sheet-current density $\tilde{K}_{Z\phi}$, and polynomial g_{Zz} (multiplied by 3) vs $u = \rho/b$ for the zero-flux-quantum state with $\tilde{a} = a/b = 0.5$.

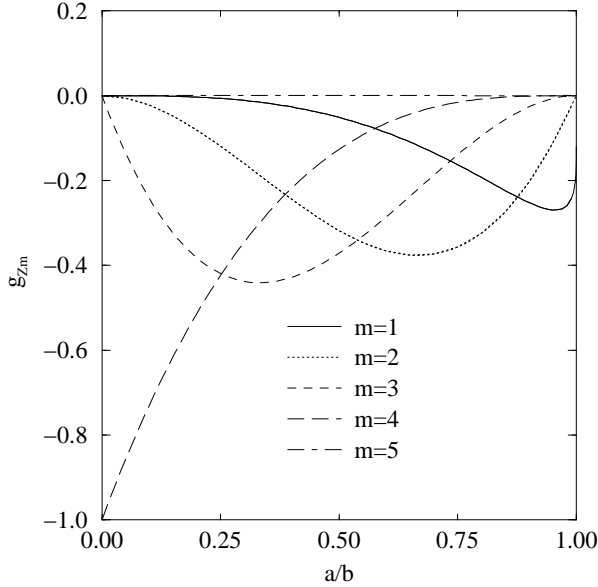


FIG. 5: Coefficients g_{Zm} in the polynomial of Eq. (23) vs $\tilde{a} = a/b$ for the zero-flux-quantum state.

We wish to determine how much magnetic flux is focused into the hole in the middle of the ring. The sheet current density in this case is $K_{F\phi} = H_a \tilde{K}_{F\phi}$, where the subscript F henceforth labels all quantities that are specific to calculations of flux focusing. To evaluate the coeffi-

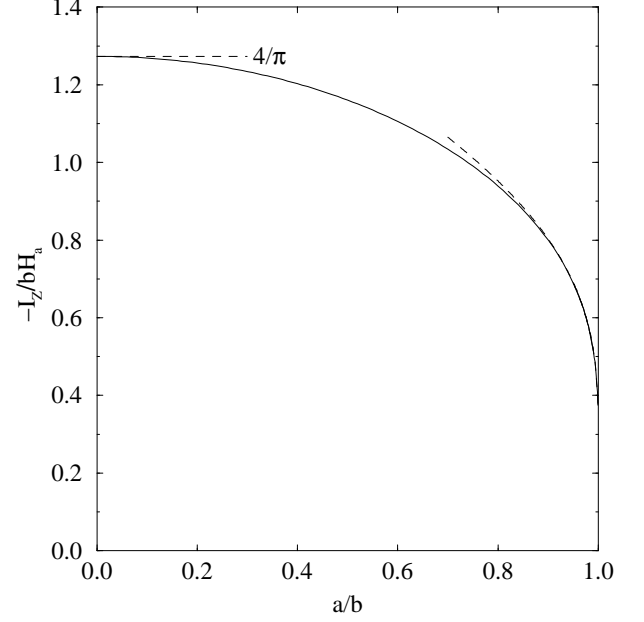


FIG. 6: Magnitude of the reduced current, $-I_Z/bH_a$, vs $\tilde{a} = a/b$ for the zero-flux-quantum state calculated from Eq. (25). Dashed curves show approximations valid in the limits $\tilde{a} \rightarrow 0$ and $\tilde{a} \rightarrow 1$.

cients g_{Fm} in

$$g_F(u) = \sum_{m=1}^N g_{Fm} \left(\frac{u - \tilde{a}}{1 - \tilde{a}} \right)^{m-1}, \quad (26)$$

we use the N equations

$$\sum_{m=1}^N \alpha_{Fnm} g_{Fm} = \beta_{Fn}, \quad (27)$$

$n = 1, 2, \dots, N$, where $\alpha_{Fnm} = \alpha_{nm}$ and $\beta_{Fn} = -1$ for $n < N$, and $\alpha_{FNm} = i_m$ and $\beta_{FN} = 0$ for $n = N$. These equations are obtained from Eqs. (1), (8), (9), (10), and (14) and $H_z(\rho_n) = 0$ for $n < N$, and from Eqs. (4), (8), (9), (11), and $I = 0$ for $n = N$.

Numerical results for $\tilde{H}_{Fz} = H_{Fz}/H_a$, $\tilde{K}_{F\phi}$, and g_F vs $u = \rho/b$ for $a = b/2$ ($\tilde{a} = 0.5$) are shown in Fig. 7. Results for g_{Fm} vs \tilde{a} are shown in Fig. 8. The magnetic flux focused into the hole is $\Phi_{Fz}(a) = \mu_0 H_a b^2 \tilde{\Phi}_{Fz}(\tilde{a})$, where

$$\tilde{\Phi}_{Fz}(\tilde{a}) = \pi \tilde{a}^2 + \sum_{m=1}^N \phi_m(\tilde{a}) g_{Fm}. \quad (28)$$

The effective area of the hole (which corresponds to the effective pickup area of a SQUID made of a circular washer), defined via $\Phi_{Fz}(a) = \mu_0 H_a A_{eff}$, is always larger than the actual area of the hole, $A_h = \pi a^2$. We find

$$\frac{A_{eff}}{A_h} = \frac{\Phi_{Fz}(a)}{\mu_0 H_a \pi a^2} = 1 + \frac{1}{\pi \tilde{a}^2} \sum_{m=1}^N \phi_m(\tilde{a}) g_{Fm}, \quad (29)$$

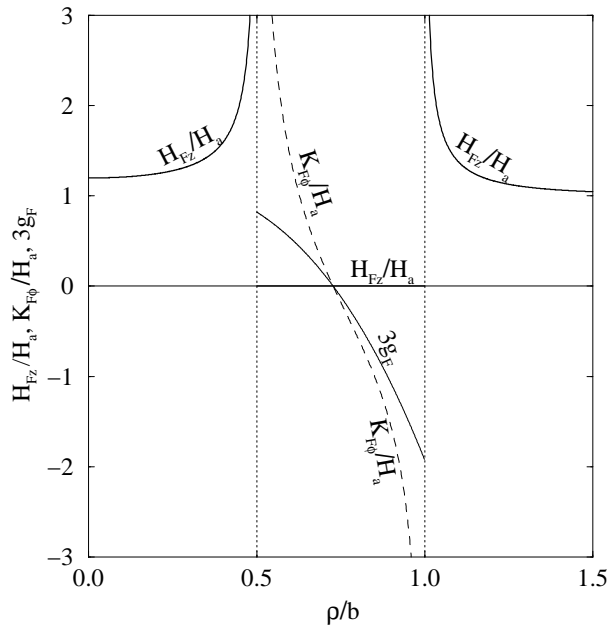


FIG. 7: Reduced magnetic field $\tilde{H}_{Fz} = H_{Fz}/H_a$, reduced sheet-current density $\tilde{K}_{F\phi}$, and polynomial g_F (multiplied by 3) vs $u = \rho/b$ for flux focusing with $\tilde{a} = a/b = 0.5$.

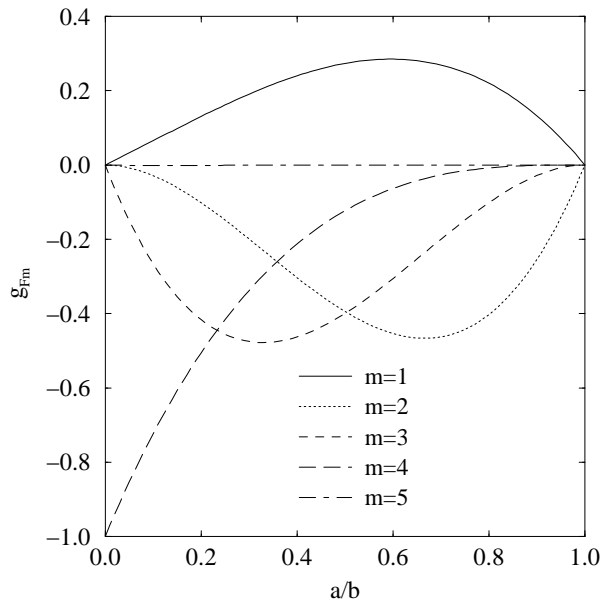


FIG. 8: Coefficients g_{Fm} in the polynomial of Eq. (26) vs $\tilde{a} = a/b$ for flux focusing.

which is shown in Fig. 9 as a function of $1/\tilde{a} = b/a$. Dashed lines in Fig. 9 show expressions valid in the limits of small and large \tilde{a} : For $\tilde{a} \ll 1$, A_{eff}/A_h approaches $(8/\pi^2)(b/a)$ [or $8/\pi^2\tilde{a}$], as obtained by Ketchen et al.,³ and for $\tilde{a} \rightarrow 1$, A_{eff}/A_h approaches $(R/a)^2$ [or $((1+\tilde{a})/2\tilde{a})^2$], where $R = (a+b)/2$ is the mean radius of the ring.

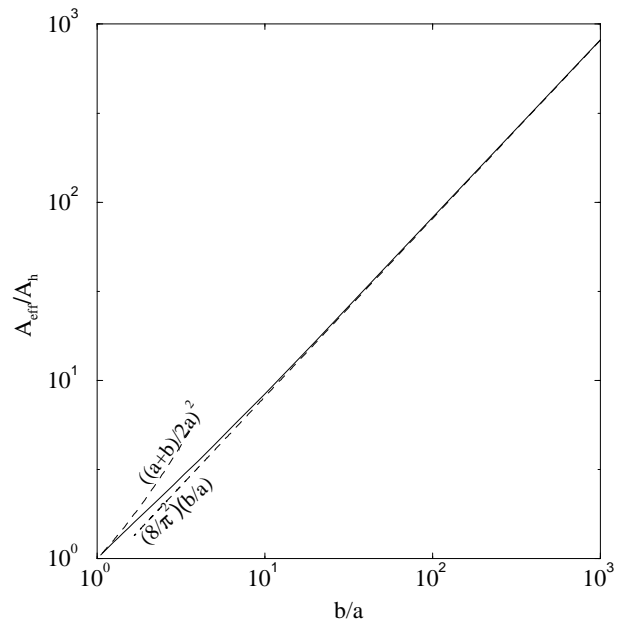


FIG. 9: Reduced effective area, A_{eff}/A_h , vs $1/\tilde{a} = b/a$ for flux focusing calculated from Eq. (29) or (30). Dashed curves show approximations valid in the limits $\tilde{a} \rightarrow 0$ and $\tilde{a} \rightarrow 1$.

The flux-focusing problem also can be solved from a linear superposition of the fields calculated in Secs. III and IV. From $K_{F\phi} = K_{I\phi} + K_{Z\phi}$ and the condition $I_F = I_I + I_Z = 0$ we obtain $g_F(u) = -\tilde{I}_Z g_I(u) + g_Z(u)$, $g_{Fm} = -\tilde{I}_Z g_{Im} + g_{Zm}$, and the result

$$\frac{A_{eff}}{A_h} = -\frac{\tilde{I}_Z \tilde{\Phi}_{Iz}(\tilde{a})}{\pi \tilde{a}^2}, \quad (30)$$

which gives numerically the same values as Eq. (29).

VI. GEOMETRICAL BARRIER

We next present an efficient method for calculating the magnetic-field and current-density distributions and the magnetization of a bulk-pinning-free type-II superconducting disk subject to a geometrical barrier, which impedes the entry of vortices into the disk. We consider a disk (radius b and thickness $d \ll b$) in the plane $z = 0$, centered on the z axis, initially in the Meissner state. We assume that the London penetration depth obeys $\lambda < d/2$ or, if $\lambda > d/2$, that the two-dimensional screening length $\Lambda = 2\lambda^2/d$ obeys $\Lambda \ll b$. When a perpendicular magnetic field H_a is applied, a sheet-current density¹³

$$K_\phi(\rho) = -\frac{4H_a}{\pi} \frac{\rho}{\sqrt{b^2 - \rho^2}} \quad (31)$$

is induced. The resulting magnetic field in the plane $z = 0$, determined from Eq. (1), is $H_z(\rho) = 0$ for $\rho < b$

and¹⁸

$$H_z(\rho) = H_a \left\{ 1 + \frac{2}{\pi} \left[\frac{1}{\sqrt{(\rho/b)^2 - 1}} - \sin^{-1}\left(\frac{b}{\rho}\right) \right] \right\} \quad (32)$$

for $\rho > b$.

A geometrical barrier prevents vortices from entering the film until the magnetic field at the edge (accounting for demagnetizing effects) reaches the value H_s . We expect that $H_s = H_{c1}$, the lower critical field, if there is no Bean-Livingston barrier, or $H_s \approx H_c$, the bulk thermodynamic critical field, if the edge is without defects and thermal activation is negligible. An equivalent criterion is that the magnetic flux begins to penetrate when the magnitude of the sheet-current density at the edge reaches the value $K_s = 2H_s$.¹⁹ To estimate H_z or K_ϕ at the edge of the film, we note that the approximations that led to Eqs. (31) and (32) break down and that the inverse-square-root divergences in these equations are cut off when ρ is within δ of the edge, where δ is the larger of $d/2$ or Λ . Accordingly, we approximate H_z at the edge of the film by replacing ρ in the square-root denominator of Eq. (32) by $b + \delta$ and using $\delta \ll b$, such that $H_z(\text{edge}) \approx (H_a/\pi)\sqrt{2b/\delta}$. Similarly, we approximate K_ϕ at the edge of the film by replacing ρ in the square-root denominator of Eq. (31) by $b - \delta$ and using $\delta \ll b$, such that $K_\phi(\text{edge}) \approx -(2H_a/\pi)\sqrt{2b/\delta}$. Whichever criterion is used [$H_z(\text{edge}) = H_s$ or $|K_\phi(\text{edge})| = K_s = 2H_s$], we estimate that the geometrical barrier is overcome when the applied field is equal to $H_0 = \pi H_s \sqrt{\delta/2b}$. (In this paper we have chosen $\tilde{\delta} = \delta/b = 0.01$, such that $H_0 = 0.222H_s$. See Fig. 13.)

When $H_a > H_0$ such that $H_z(\text{edge}) > H_s$, vortices nucleate at the edge of the disk and move rapidly towards the center of the disk under the influence of the Lorentz force per unit length, $\mathbf{f} = \mathbf{J}_H \times \vec{\phi}_0$, where $\mathbf{J}_H = \nabla \times \mathbf{H}_{rev}$, $\vec{\phi}_0$ is a vector of magnitude $\phi_0 = h/2e$ along the vortex axis, and \mathbf{H}_{rev} is the thermodynamic magnetic field in equilibrium with the magnetic flux density \mathbf{B} inside the superconductor. As more vortices enter, the return field outside the disk generated by the vortices inside the disk gradually reduces the value of the field at the edge to H_s , thereby halting further vortex nucleation. If bulk pinning is negligible, the case considered in this paper, the vortices adjust their positions such that the magnetic flux density (averaged over the intervortex distance) in the plane of the disk $B_z(\rho)$ has its maximum value at the center, decreases monotonically to zero at $\rho = a$, and remains zero for $a < \rho < b$. The corresponding sheet current density $K_{H\phi} = J_{H\phi}d$ is zero for $\rho \leq a$, such that the Lorentz force on any vortex vanishes and no further motion occurs. Screening supercurrents still flow, however, in the vortex-free region $a < \rho < b$.

To good approximation when $d \ll b$, the resulting magnetic-field and supercurrent distributions are the same as those generated by a thin superconducting annular ring ($a < \rho < b$) in a perpendicular applied field H_a , when the solutions are subject to the constraint that

the sheet current density K_ϕ is zero at $\rho = a$. The Biot-Savart law [Eq. (1) and its extension to $|z| > 0$] guarantees that the current density $\mathbf{J}_B = \nabla \times \mathbf{B}/\mu_0$ is zero everywhere except within the ring $a < \rho < b$; thus $K_{B\phi} = J_{B\phi}d$ is zero for $\rho \leq a$. Because \mathbf{J}_H and \mathbf{J}_B in thin films are dominated by the curvature of \mathbf{H}_{rev} and \mathbf{B}/μ_0 , rather than by the gradients ∇H_{rev} and $\nabla B/\mu_0$,^{9,20} it can be shown that the difference between $K_{H\phi}$ and $K_{B\phi}$ is of order $(d/b)H_a$, decreases for $B > 2B_{c1}$ as \mathbf{H}_{rev} approaches \mathbf{B}/μ_0 , and is negligible for the thin films considered in this paper ($d/b = 0.01$). Nevertheless, our simplified approach would be incapable of calculating details in the structure that has been observed in the magnetic flux-density distribution at the vortex-lattice melting transition.²¹ To treat such a problem would require a more refined approach such as that in Refs. 12 and 22, which calculates the local \mathbf{J}_B currents flowing at the vortex solid-liquid interface and distinguishes between \mathbf{H}_{rev} and \mathbf{B}/μ_0 .

The magnetic-field and supercurrent distributions for the case of a thin pin-free disk subject to a geometrical barrier therefore can be calculated efficiently by using an approach similar to that used in Secs. II-V. When a Lorenz-force-free dome of magnetic flux occupies the region $\rho < a$, the sheet current density in the region $a < \rho < b$ is $K_{G\phi} = H_a \tilde{K}_{G\phi}$, where the subscript G hencefore labels all quantities that are specific to the geometrical-barrier problem. To evaluate the coefficients g_{Gm} in

$$g_G(u) = \sum_{m=1}^N g_{Gm} \left(\frac{u - \tilde{a}}{1 - \tilde{a}} \right)^{m-1}, \quad (33)$$

we use the N equations

$$\sum_{m=1}^N \alpha_{Fnm} g_{Gm} = \beta_{Gn}, \quad (34)$$

$n = 1, 2, \dots, N$, where $\alpha_{Gnm} = \alpha_{nm}$ and $\beta_{Gn} = -1$ for $n < N$, and $\alpha_{GNm} = \delta_{1m}$ and $\beta_{GN} = 0$ for $n = N$. These equations are obtained from Eqs. (1), (8), (9), (10), and (14) and $H_z(\rho_n) = 0$ for $n < N$, and from Eqs. (8), (9), and $\tilde{K}_{G\phi}(\tilde{a}) = 0$ for $n = N$.

Numerical results for $\tilde{H}_{Gz} = H_{Gz}/H_a$, $\tilde{K}_{G\phi}$, and g_G vs $u = \rho/b$ for $a = b/2$ ($\tilde{a} = 0.5$) are shown in Fig. 10. In these calculations, we have made no distinction between \mathbf{H}_{rev} and \mathbf{B}/μ_0 , which corresponds to assuming that $B \approx \mu_0 H$. However, in cases for which B differs significantly from $\mu_0 H$, our plots of H_{Gz}/H_a (such as in Fig. 10) would correspond most closely to plots of the reduced flux density B_{Gz}/B_a . Results for g_{Gm} vs \tilde{a} are shown in Fig. 11. The magnetic flux contained within $\rho < a$ can be obtained from

$$\Phi_{Gz}(a) = \mu_o H_a b^2 \tilde{\Phi}_{Gz}(\tilde{a}), \quad (35)$$

where

$$\tilde{\Phi}_{Gz}(\tilde{a}) = \pi \tilde{a}^2 + \sum_{m=1}^N \phi_m(\tilde{a}) g_{Gm}, \quad (36)$$

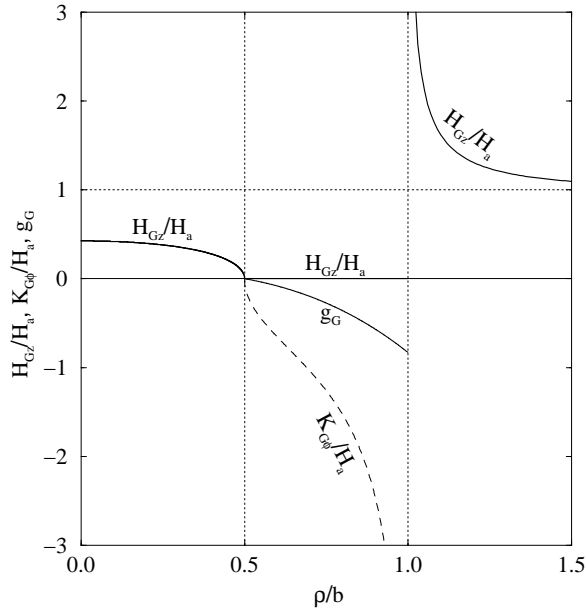


FIG. 10: Reduced magnetic field $\tilde{H}_{Gz} = H_{Gz}/H_a$, reduced sheet-current density $\tilde{K}_{G\phi}$, and polynomial g_G vs $u = \rho/b$ for a pin-free disk of radius b with a geometrical barrier and a flux dome of reduced radius $\tilde{a} = a/b = 0.5$.

and the average magnetic flux density in the disk is $B_{av} = \Phi_{Gz}(a)/\pi b^2$. Figure 12 shows how B_{av}/B_a and $H_{Gz}(0)/H_a$, where $H_{Gz}(0)$ is the magnetic field at the center of the disk, depend upon \tilde{a} .

We next calculate the magnetization, i.e., the magnetic moment per unit volume of the disk, $M_{Gz} = m_{Gz}/\pi b^2 d$, where m_{Gz} is calculated from Eq. (5). The initial magnetization of the disk in the Meissner state ($0 \leq H_a \leq H_0$, see Fig. 13), calculated from Eq. (31), is²³ $M_{Gz} = -\chi_0 H_a$, where $\chi_0 = 8b/3\pi d$; i.e., the external magnetic susceptibility²⁴ in this case is $\chi = -\chi_0$. Whenever there is a dome of magnetic flux within the region $\rho < a$, the magnetization, obtained from Eqs. (5), (8), (12), and (33), may be calculated from

$$M_{Gz} = \frac{3\pi}{8} \chi_0 H_a \sum_{m=1}^N f_m g_{Gm}, \quad (37)$$

where f_m and g_{Gm} depend implicitly upon \tilde{a} .

For $H_0 < H_a < H_{irr}$ along the field-increasing magnetization curve at the critical entry condition (see Fig. 13), H_a and \tilde{a} are related via

$$H_a = -H_0 \sqrt{1 - \tilde{a}^2} / \sum_{m=1}^N g_{Gm}, \quad (38)$$

This equation follows from the condition that $|K_{G\phi}(\text{edge})| = 2H_s$, where $K_{G\phi}(\text{edge})$ is obtained by evaluating Eq. (8) at $u = 1$ but replacing $\sqrt{1 - u^2}$ in the denominator by $\sqrt{2\delta/b}$, as in the evaluation of H_0 . When $\tilde{a} = 0$, we see by comparing

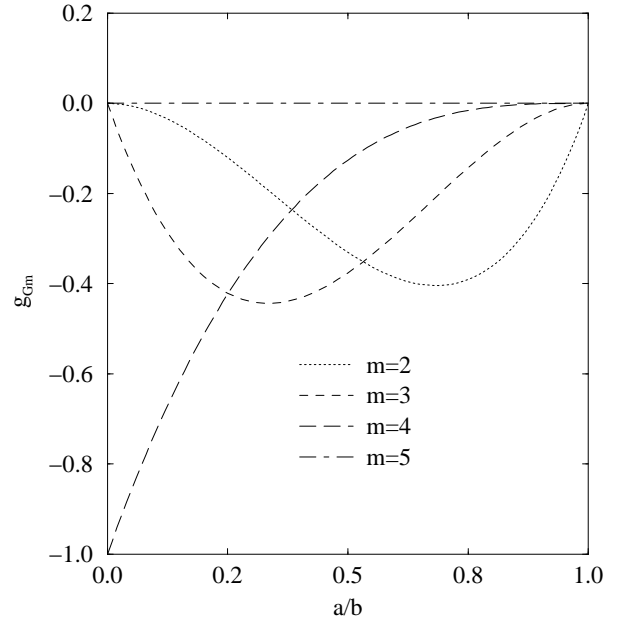


FIG. 11: Coefficients g_{Gm} in the polynomial of Eq. (33) vs \tilde{a} for a pin-free disk of radius b with a geometrical barrier and a flux dome of reduced radius $\tilde{a} = a/b$. We require $g_{G1} = 0$.

Eqs. (8) and (31) that $g_G(u) = -u^3$, such that $g_{Gm} = -\delta_{m4}$ (see also Fig. 11), $f_4 = 8/3\pi$, and $M_{Gz\uparrow} = -\chi_0 H_0$ at $H_a = H_0$. In the limit as $\tilde{a} \rightarrow 1$, $\tilde{K}_{G\phi} \approx -2\sqrt{u - \tilde{a}}/\sqrt{1 - u}$, such that $g_G(u) \approx -\pi(u - \tilde{a})$, $g_{Gm} \approx -\pi(1 - \tilde{a})\delta_{m2}$, $f_2 \approx 1$, $H_a \approx H_0\sqrt{2}/\pi\sqrt{1 - \tilde{a}}$, and $M_{Gz\uparrow}/\chi_0 H_s \approx -(3\pi^2/8)\tilde{\delta}H_s/H_a$, where $\tilde{\delta} = \delta/b \ll 1$.

For $H_0 < H_a < H_{irr}$ along the field-decreasing magnetization curve at the critical exit condition, we assume that the radius a of the vortex-filled region has reached within δ of the radius b of the disk; i.e., $\tilde{a} = 1 - \tilde{\delta}$. Using Eq. (37) with $g_{Gm} \approx -\pi\tilde{\delta}\delta_{m2}$ and $f_2 \approx 1$, we obtain $M_{Gz\downarrow}/\chi_0 H_s \approx -(3\pi^2/8)\tilde{\delta}H_a/H_s$. See Fig. 13.

The field-increasing and field-decreasing magnetization curves in Fig. 13 meet at $H_a = H_{irr}$, the irreversibility field. The criteria we used for the critical entry and exit conditions lead to the result that $H_{irr} \approx H_s$, where the magnetization is given by $M_{Gzirr}/\chi_0 H_s \approx -(3\pi^2/8)\tilde{\delta}$. However, the above expressions for H_{irr} , M_{Gzirr} , and $M_{Gz\downarrow}$ are the least reliable results of our paper, because all these quantities are very sensitive to the precise conditions for entry and exit at the edge of the disk, including such details as the shape of the edge.^{7,8,9,10,12,22} The magnetic moment responsible for the magnetization M_{Gzirr} and $M_{Gz\downarrow}$ is produced by currents that flow only within a very narrow band around the disk's edge, where a theory more accurate than ours is needed.

The minor hysteresis “loop,” shown as the dashed curve in Fig. 13, can be calculated as follows. We start at a point on the field-increasing magnetization curve where the flux dome has radius a_1 . The magnetic flux contained within the dome $\Phi_{Gz}(a_1)$, the magnetization

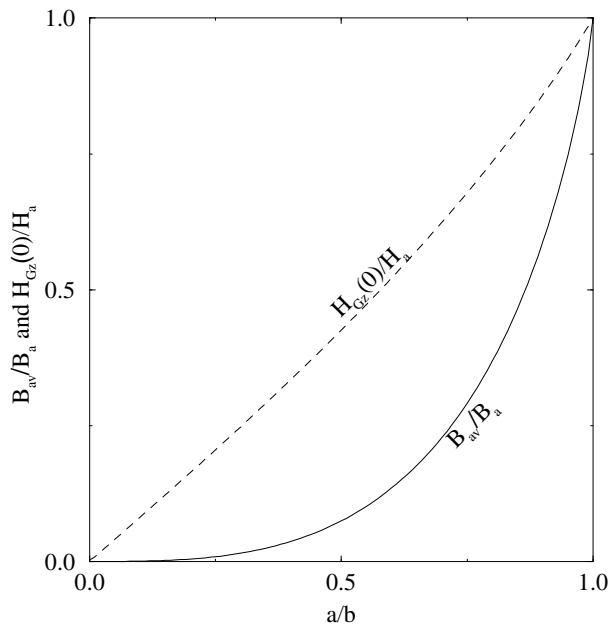


FIG. 12: Reduced average flux density B_{av}/B_a (solid) and reduced flux density at the center $H_{Gz}(0)/H_a$ (dashed) of a pin-free disk of radius b with a geometrical barrier and a flux dome of reduced radius $\tilde{a} = a/b$.

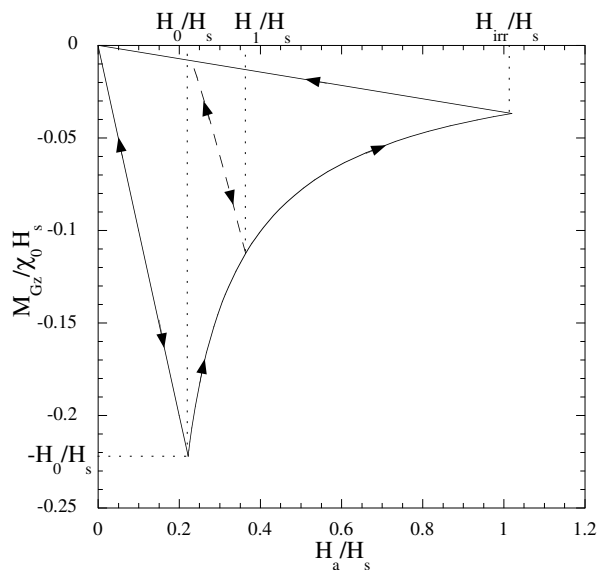


FIG. 13: Calculated hysteresis in the reduced magnetization $M_{Gz}/\chi_0 H_s$ vs reduced applied field H_a/H_s for a pin-free disk with a geometrical barrier (solid). The dashed curve shows a reversible minor hysteresis “loop” occurring when the applied field is reduced after the applied field H_a has reached H_1 along the field-increasing magnetization curve. As H_a decreases, the flux dome expands, but the flux contained within the dome remains constant.

M_{Gz1} , and the corresponding applied field H_1 are obtained from Eqs. (35), (37), and (38), where \tilde{a} , f_m , and g_{Gm} are all evaluated at $\tilde{a} = \tilde{a}_1 = a_1/b$. As the applied field H_a is reduced from its starting value H_1 , the radius a of the flux dome expands, but the magnetic flux within the dome remains constant. For each value of $\tilde{a} > \tilde{a}_1$, we recalculate f_m , g_{Gm} , and $\tilde{\Phi}_{Gz}(\tilde{a})$. We then use Eq. (35) to obtain the corresponding value of the applied field,

$$H_a = H_1 \tilde{\Phi}_{Gz}(\tilde{a}_1) / \tilde{\Phi}_{Gz}(\tilde{a}), \quad (39)$$

and Eq. (37) to obtain the corresponding value of the magnetization.

VII. DISCUSSION

In this paper, we have presented an efficient method for the calculation of magnetic-field and current-density profiles for thin-film rings in the Meissner state and for bulk-pinning-free disks subject to a geometrical barrier. In each case, the sheet-current density was expressed in the form of Eq. (8), where the quantity $g(u)$ in the numerator is a polynomial of degree $N - 1$.

For all the calculations presented in the figures, for which we assumed $N = 5$, we found that the magnitude of g_5 was less than 0.0012 in each case (see Figs. 2, 5, 8, and 11) and that its contribution to $g(u)$ was less than 1.1%. Using $N = 6$ yields values of g_6 whose magnitudes are much smaller than those of g_5 , and the values of the calculated physical quantities are altered only in the sixth decimal place.

Moreover, we offer the conjecture that the problems we solved numerically in Secs. III-VI might be solved analytically with functions g_I, g_Z, g_F , and g_G that are third-order polynomials in u ; i.e., the sums in Eqs. (9), (16), (23), (26), and (33) might simply terminate with $N = 4$. As evidence in support of this conjecture, we note that our calculations for $\tilde{a} = a/b = 0.1$ and 0.5 with $N = 4, 5, 6$, and 7 yielded values of $L/\mu_0 b$ [Eqs. (18) and (19)] that differed only in the fifth decimal place. Similarly, values of $I_Z/H_a b$ [Eq. (25)], A_{eff}/A_h [Eq. (29)], and $M_{Gz\uparrow}/\chi_0 H_s$ [Eqs. (37) and (38)] calculated for $\tilde{a} = a/b = 0.1$ and 0.5 with $N = 4, 5, 6$, and 7 differed at most only in the fourth significant figure. It is possible that the values we obtained for g_5, g_6 , and g_7 in Secs. III-VI were nonzero only because of small numerical errors introduced because we performed the integrals in Eqs. (10)-(13) numerically rather than analytically.

Although in this paper we have considered only bulk-pinning-free thin-film rings and disks, it should be possible to extend the present approach to develop an efficient method, complementary to that of Ref. 6, for numerically calculating quasistatic magnetic-field and current-density distributions in rings and disks subject to both a geometrical barrier and bulk pinning. Such distributions recently have been calculated analytically for infinitely long strips in Refs. 11,25,26,27,28.

Acknowledgments

We thank J. Clarke and V. G. Kogan for stimulating discussions. This manuscript has been authored in

part by Iowa State University of Science and Technology under Contract No. W-7405-ENG-82 with the U.S. Department of Energy.

-
- ¹ A. A. Babaei Brojeny, Y. Mawatari, M. Benkraouda, and J. R. Clem, *Supercond. Sci. Technol.* **15**, 1454 (2002).
- ² M. B. Ketchen and J. M. Jaycox, *Appl. Phys. Lett.* **40**, 736 (1982).
- ³ M. B. Ketchen, W. J. Gallagher, A. W. Kleinsasser, S. Murphy, and J. R. Clem, in *SQUID '85, Superconducting Quantum Interference Devices and their Applications*, edited by H. D. Hahlbohm and H. Lübbig (de Gruyter, Berlin, 1985), p. 865.
- ⁴ E. Dantsker, S. Tanaka, and J. Clarke, *Appl. Phys. Lett.* **70**, 2037 (1997).
- ⁵ A.B.M. Jansman, M. Izquierdo, A. Eiguren, J. Flokstra, and H. Rogalla, *Appl. Phys. Lett.* **72**, 3151 (1998).
- ⁶ J. Gilchrist and E. H. Brandt, *Phys. Rev. B* **54**, 3530 (1996).
- ⁷ Th. Schuster, M. V. Indenbom, H. Kuhn, E. H. Brandt, and M. Konczykowski, *Phys. Rev. Lett.* **73**, 1424 (1994).
- ⁸ E. Zeldov, A. I. Larkin, V. B. Geshkenbein, M. Konczykowski, D. Majer, B. Khaykovich, V. M. Vinokur, and H. Shtrikman, *Phys. Rev. Lett.* **73**, 1428 (1994).
- ⁹ M. Benkraouda and J. R. Clem, *Phys. Rev. B* **53**, 5716 (1996).
- ¹⁰ Y. Mawatari and J. R. Clem, *Phys. Rev. B* **68**, 049326 (2003).
- ¹¹ I. L. Maksimov and A. A. Elistratov, *Appl. Phys. Lett.* **72**, 1650 (1998).
- ¹² T. B. Doyle, R. Labusch, and R. A. Doyle, *Physica C* **290**, 148 (1997).
- ¹³ L. D. Landau and E. M. Lifshitz, *Electrodynamics of Continuous Media* (Addison-Wesley, Reading, 1960).
- ¹⁴ J. D. Jackson, *Classical Electrodynamics* (Wiley, New York, 1962).
- ¹⁵ E. H. Brandt, *Phys. Rev. B* **55**, 14513 (1997).
- ¹⁶ C. P. Poole, Jr., H. A. Farach, and R. J. Creswick, *Superconductivity* (Academic Press, San Diego, 1995).
- ¹⁷ Similarly, the inductance per unit length [Eq. (17) of Ref. 1] of a pair of parallel coplanar superconducting strips of center-to-center distance s and strip-width w approaches $L'_0 = (\mu_0/\pi) \ln(4s/w)$ when $w \ll s$, which can be obtained from $L' = (\mu_0/\pi) \ln(s/r)$, the inductance per unit length of a pair of superconducting wires of center-to-center distance s and radius r , by replacing r by $w/4$.
- ¹⁸ P. N. Mikheenko and Yu. E. Kuzovlev, *Physica C* **204**, 229 (1993).
- ¹⁹ M. Yu. Kupriyanov and K. K. Likharev, *Fiz. Tverd. Tela* **16**, 2829 (1974) [*Sov. Phys. Solid State* **16**, 1835 (1975)].
- ²⁰ J. Frankel, *J. Appl. Phys.* **50**, 5402 (1979).
- ²¹ A. Soibel, E. Zeldov, M. Rappaport, Y. Myasoedov, T. Tamegai, S. Ooi, M. Konczykowski, and V. B. Geshkenbein, *Nature* **406**, 282 (2000).
- ²² R. B. Doyle, R. Labusch, and R. A. Doyle, *Physica C* **332**, 365 (2000).
- ²³ J. R. Clem and A. Sanchez, *Phys. Rev. B* **50**, 9355 (1994).
- ²⁴ R. B. Goldfarb, M. Leental, and C. A. Thompson, in *Magnetic Susceptibility of Superconductors and Other Spin Systems*, R. A. Hein, T. L. Francavilla, and D. H. Liebenberg, eds. (Plenum Press, New York, 1992), p. 49.
- ²⁵ A. A. Elistratov and I. L. Maksimov, *Phys. Solid State* **42**, 201 (2000).
- ²⁶ N. V. Zhelezina and G. M. Maksimova, *Tech. Phys. Lett.* **28**, 618 (2002).
- ²⁷ I. L. Maksimov and A. A. Elistratov, *Appl. Phys. Lett.* **80**, 2701 (2002).
- ²⁸ A. A. Elistratov, D. Yu. Vodolazov, I. L. Maksimov, and J. R. Clem, *Phys. Rev. B* **66**, 220506(R) (2002); erratum *Phys. Rev. B* **67**, 099901(E) (2003).